AGU100 ADVANCING EARTH AND SPACE SCIENCE

Geochemistry, Geophysics, Geosystems

RESEARCH ARTICLE
10.1029/2018GC007464

Key Points:
- HyMaTZ calculates seismic velocity profiles for different states of hydration in the transition zone
- In the upper MTZ, adding 1.65 wt% H_2O, 7 mol% Fe, or increasing temperature by 160 K cause roughly equivalent reductions in V_S
- Velocities within the eastern U.S. low-velocity anomaly are consistent with ~1 wt% H_2O in wadsleyite along a 1600 K adiabat

Correspondence to:
F. Wang,
feiwang2020@u.northwestern.edu

Citation:
Wang, F., Barklage, M., Lou, X., van der Lee, S., Bina, C. R., & Jacobsen, S. D. (2018). HyMaTZ: A Python program for modeling seismic velocities in hydrous regions of the mantle transition zone. *Geochemistry, Geophysics, Geosystems*, *19*, 2308–2324. https://doi.org/10.1029/2018GC007464

Received 30 JAN 2018
Accepted 25 JUN 2018
Accepted article online 27 JUL 2018
Published online 4 AUG 2018

HyMaTZ: A Python Program for Modeling Seismic Velocities in Hydrous Regions of the Mantle Transition Zone

Fei Wang[1], Mitchell Barklage[1], Xiaoting Lou[1], Suzan van der Lee[1], Craig R. Bina[1], and Steven D. Jacobsen[1]

[1]Department of Earth and Planetary Sciences, Northwestern University, Evanston, IL, USA

Abstract Mapping the spatial distribution of water in the mantle transition zone (MTZ, 410- to 660-km depth) may be approached by combining thermodynamic and experimental mineral physics data with regional studies of seismic velocity and seismic discontinuity structure. HyMaTZ (Hydrous Mantle Transition Zone) is a Python program with graphical user interface, which calculates and displays seismic velocities for different scenarios of hydration in the MTZ for comparison to global or regional seismic-velocity models. The influence of water is applied through a regression to experimental data on how H_2O influences the thermoelastic properties of $(Mg,Fe)_2SiO_4$ polymorphs: olivine, wadsleyite, and ringwoodite. Adiabatic temperature profiles are internally consistent with dry phase proportion models; however, modeling hydration in HyMaTZ affects only velocities and not phase proportions or discontinuity structure. For wadsleyite, adding 1.65 wt% H_2O or increasing the iron content by 7 mol% leads to roughly equivalent reductions in V_S as raising the temperature by 160 K with a pyrolite model in the upper part of the MTZ. The eastern U.S. low-velocity anomaly, which has been interpreted as the result of dehydration of the Farallon slab in the top of the lower mantle, is consistent with hydration of wadsleyite to about 20% of its water storage capacity in the upper MTZ. Velocity gradients with depth in absolute shear velocity models are steeper in all seismic models than all mineralogical models, suggesting that the seismic velocity gradients should be lowered or varied with depth and/or an alternative compositional model is required.

Plain Language Summary Olivine and its high-pressure polymorphs, wadsleyite and ringwoodite, constitute at least half of the material in the Earth's upper mantle. In addition to magnesium, iron, silicon, and oxygen, these phases are known for their ability to incorporate H_2O. Water is incorporated into their crystal structures as OH (hydroxyl) defects, charge-balanced primarily by cation vacancies. Hydration of olivine, wadsleyite, and ringwoodite through such defects modifies their density and elastic properties such as the bulk (K) and shear (G) moduli, which can lead to changes in seismic velocities as determined from analyses of seismograms using methods such as seismic tomography. This paper presents a tool for researchers to calculate and graph the influence of hydration in olivine, wadsleyite, and ringwoodite for comparison to any seismic-velocity model. While Hydrous Mantle Transition Zone accounts for elastic property changes due to hydration, the effect of water on thermodynamic phase proportions is not yet included. The goal of such studies is to assess the amount and regional distribution of water in the mantle transition zone.

1. Introduction

Seismic tomography is an imaging technique used to map three-dimensional variations in the seismic-velocity structure of the Earth's interior at global (e.g., French & Romanowicz, 2014; Grand, 2002; Ritsema et al., 2004; Van der Hilst et al., 1997) or regional scales (e.g., Barklage et al., 2015; Bedle & Van der Lee, 2009; Burdick et al., 2017; Schmandt & Lin, 2014; Van der Lee & Frederiksen, 2005). Regional variations in velocity structure are always relative to one-dimensional seismic velocity profiles that change only with depth. Interpretations of observed seismic velocity variations require mineralogical models of the Earth's mantle obtained by phase equilibria and thermoelastic properties of major minerals as a function of pressure, temperature, and composition (Goes & Van der Lee, 2002; Li & Liebermann, 2007; Stixrude & Lithgow-Bertelloni, 2012; Wang et al., 2015; Wood, 1995; Xu et al., 2008).

The pyrolite model of the upper mantle and transition zone is composed of ~60% by volume of $(Mg,Fe)_2SiO_4$ polymorphs, olivine, wadsleyite, and ringwoodite (Irifune & Ringwood, 1987; Ringwood & Major, 1967). These phases are nominally anhydrous minerals (NAMs) but may contain up to several weight percent of H_2O as

hydroxyl defects in their structure (Bolfan-Casanova, 2005; Kohlstedt et al., 1996; Smyth, 1987, 1994). Incorporation of water into NAMs, accompanied by Mg^{2+} point defect vacancies, strongly influences their elastic properties (e.g., Jacobsen, 2006, Mao & Li, 2016) suggesting that the velocity structure of the mantle transition zone (MTZ) may be used to model mantle water content (Thio et al., 2016; Van der Lee et al., 2008).

Whereas some studies suggest efficient dehydration of downgoing slabs in the mantle (e.g., Green et al., 2010), the finding of 1.5 wt% H_2O in a natural ringwoodite inclusion in diamond (Pearson et al., 2014) provides evidence that regions of the MTZ where some superdeep diamonds may derive are very hydrous. Regional-scale seismic studies suggest variable water content of the MTZ (Courtier & Revenaugh, 2006; Emry et al., 2015; Liu et al., 2016; Schmandt et al., 2014; Van der Lee et al., 2008; Van der Meijde et al., 2003); however, recent viscosity measurements of hydrated ringwoodite suggest a globally saturated transition zone (Fei et al., 2017). Evaluating the regional-scale water content of the MTZ is important to understanding Earth's deep water cycle (Hirschmann, 2006; Jacobsen & Van der Lee, 2006; Karato, 2011; Ohtani et al., 2004).

Although the thermodynamic properties of hydrous phases in the deep mantle, especially dense hydrous magnesium silicates, have been thoroughly investigated (e.g., Frost, 2006, Komabayashi & Omori, 2006, Ohtani et al., 2001), the influence of water on phase equilibria in NAMs is largely experimental (e.g., Chen et al., 2002, Frost & Dolejš, 2007, Smyth & Frost, 2002). Thermodynamic databases for calculating phase equilibria treat H_2O as a chemical component in hydrous phases but do not account for water in NAMs (Connolly, 2005; Cottaar et al., 2014; Holland et al., 2013). On the other hand, numerous laboratory studies have been conducted on the influence of water on elastic properties of olivine (Jacobsen et al., 2008; Mao et al., 2010), wadsleyite (Chang et al., 2015; Mao et al., 2008, 2011), and ringwoodite (Jacobsen & Smyth, 2006; Mao et al., 2012; Wang et al., 2006).

In this work, we develop a graphical user interface for a computational tool called Hydrous Mantle Transition Zone (HyMaTZ), written in Python, to evaluate the influence of water on predicted seismic velocities in the MTZ. Phase proportions for various compositional models are calculated using Perple_X (Connolly, 2005) along adiabatic temperature gradients specified by the user. If a dry compositional model is chosen, the thermodynamic data from Perple_X are applied. However, if one provides a water content depth profile, experimental constraints on the influence of H_2O on elastic properties are applied through a regression to the provided experimental laboratory database. One can also input a custom variation of elastic properties and density with water content. At this stage, because there is no thermodynamic database for H_2O in NAMs, the phase proportions used by HyMaTZ are not affected by water. In this way, HyMaTZ allows one to explore the influence of water on bulk compressional (V_P) and shear wave velocity (V_S) in the depth range of ~300–700 km for comparison to regional or global seismic velocity models. In this paper, some example uses of HyMaTZ are shown, and it is demonstrated that increasing the water content of the upper MTZ by 1.65 wt% H_2O in wadsleyite has about the same influence on V_S as increasing the iron content by ~7 mol% or raising the temperature by 160 K.

2. Methods

2.1. Thermoelastic Properties

Three independent physical parameters, namely, density (ρ), adiabatic bulk modulus (K_S), and shear modulus (G), are required to calculate the seismic velocities

$$V_P = \sqrt{\frac{K_S + \left(\frac{4}{3}\right)G}{\rho}} \tag{1}$$

$$V_S = \sqrt{\frac{G}{\rho}} \tag{2}$$

where V_P and V_S are the P wave and S wave velocities, respectively. In order to calculate the density, bulk modulus, and shear modulus of a polymineralic rock, one requires elastic properties of all the individual components, either experimentally or computationally derived, an equation of state (EOS) that describes the variation of elastic properties with pressure and temperature, and a polycrystalline averaging scheme that

distributes stress or strain uniformly across all grains. In addition, the compositional sensitivity of thermoelastic properties requires thermodynamic or experimental input. In this work, the thermoelastic properties of all the anhydrous minerals are derived from the output of Perple_X from a variety of referenced compositional models.

2.1.1. Internally Consistent Thermodynamic Data Set

In order to calculate the thermoelastic properties of minerals at mantle conditions, a thermodynamic database and equations of state appropriate for the desired range of pressures and temperatures are essential. An assessment of phase equilibria calculations for mantle rock compositions as a function of pressure and temperature using Perple_X gives consistent results with observations (Connolly, 2009). The work of establishing a self-consistent database fitted to many different types of thermodynamic experiments has been an iterative process. The database published by Stixrude and Lithgow-Bertelloni (2011) was developed by requiring that all data satisfy self-consistency of fundamental thermodynamics relationships, and it is appropriate for use in the current work because the data set provides a rigorous baseline for dry compositions.

2.1.2. Equation of State

The high *P-T* conditions of the transition zone require the use of a thermodynamic EOS to interpolate and extrapolate the available experimental data to those conditions. For HyMaTZ, we have chosen to use the third-order Birch-Murnaghan formalism with the Mie-Grüneisen-Debye temperature correction developed by Stixrude and Lithgow-Bertelloni (2005). This has also been shown to give good results in calculating phase equilibria in the Earth's mantle (Stixrude & Lithgow-Bertelloni, 2011).

To calculate the thermoelastic properties of each mineral across *P-T* conditions of the MTZ, a total of 11 parameters are used in the EOS model (Stixrude & Lithgow-Bertelloni, 2005, 2011). Referring to equation (1), the adiabatic modulus K_S is used, whereas the internally consistent thermodynamic data set uses the isothermal bulk modulus, K_T. We obtain K_S from K_T using the following relation:

$$K_S = K_T(1 + \gamma\alpha T) \tag{3}$$

where γ is the Grüneisen parameter and α is the coefficient of thermal expansion, related by

$$\alpha = \frac{\gamma C_V \rho}{K_T} \tag{4}$$

where ρ is density and C_V is the isochoric heat capacity. Detailed explanation of the EOS and its application are given in Stixrude and Lithgow-Bertelloni (2005) and by Cottaar et al. (2014).

2.1.3. Mineral Phase Proportion Models

HyMaTZ uses the output of Perple_X (Connolly, 2005) for obtaining thermodynamic quantities and phase proportions of the minerals at mantle conditions. Perple_X implements the EOS described above and Gibbs-free energy minimization to calculate the equilibrium mineral phases as a function of chemical composition, pressure, and temperature. Six oxides are used to define the bulk chemical composition: CaO, FeO, MgO, Al_2O_3, SiO_2, and Na_2O, which can comprise 47 phases (Stixrude & Lithgow-Bertelloni, 2011). Once the user specifies the foot temperature at the Earth's surface for an adiabatic temperature profile, HyMaTZ accesses an included data file containing the phase equilibria (mineral proportions and compositions) as well as the thermodynamics variables (e.g., entropy and density) at each *P-T* point on a 2-D grid with the pressure range of 0–30 GPa and from 773–2773 K. The model is composed of 600 nodes on the pressure axis and 400 nodes on the temperature axis. For the purpose of plotting a more precise phase proportion model, parameters at *P-T* points in between nodes are obtained by linear interpolation. Because mantle temperatures above ~300-km depth are not adiabatic and are highly region dependent, the results of HyMaTZ are most valid for the 300- to 700-km range.

HyMaTZ includes data files from Perple_X for four compositional models: pyrolite, basalt, and harzburgite from Xu et al. (2008) and piclogite from Weidner (1986). Phase proportions and thermodynamic data are extracted from these data files along the user-specified adiabat (section 2.1.4). A list of the compositional models included in HyMaTZ is shown in Table 1. In addition to these models, HyMaTZ includes fixed percentage mixtures of harzburgite and basalt at 90/10, 80/20, 70/30, 60/40, 50/50, 40/60, 30/70, 20/80, and 10/90 of harzburgite/basalt, where the ratios give their molar compositional proportions input to Perple_X. In addition to these models composed of equilibrated compositional mixtures of harzburgite and basalt, the user can

Table 1
End-Member Compositional Models Included With HyMaTZ

Model	Reference	Oxide (wt%)					
		SiO_2	MgO	FeO	Na_2O	Al_2O_3	CaO
Pyrolite	Xu et al. (2008)	44.93	38.83	8.57	0.13	4.36	3.18
Harzburgite	Xu et al. (2008)	43.52	45.73	8.76	0	1.09	0.91
Basalt	Xu et al. (2008)	50.39	9.76	8.22	2.19	16.84	12.61
Piclogite	Weidner (1986)	48.91	21.01	5.69	3.00	14.39	7.00

work with a nonequilibrated mechanical mixture of any two end-member models in any percentage. By mechanical mixing we mean that the output phase proportions and thermodynamic properties are averaged according to the volume proportions of each, specified by the user.

2.1.4. Pressure and Temperature

In preparation for running a velocity model calculation with HyMaTZ, we include the capability to calculate self-consistent pressures and isentropic temperatures in a 1-D column in the Earth, which is divided into 300 nodes. The calculation begins at the first node by calculating the density at 1 bar and at a foot temperature provided in step 2 by the user specifying the isentropic potential temperature at the Earth's surface. The pressure-depth profile along the user-specified adiabat is obtained iteratively with

$$dP = \rho(r)g(r)dr \tag{5}$$

where P is pressure, ρ is the average density between two nodes, g is the acceleration due to gravity, and r is radius from the Earth's center. The next pressure is calculated by initially taking the density at the next node to be the same as at the previous node, calculating the overburden pressure (equation (5)), and then updating the pressure to calculate the next value of density. From the pressure, temperature is determined from the output of Perple_X (included in the Models folder) using the requirement that the two nodes have the same entropy. Finally, the process is iterated until the density difference between two consecutive iterations is less than 0.01 kg/m^3, which usually converges in two or three steps, as previously reported by Afonso et al. (2008).

2.1.5. Averaging Schemes for Polycrystalline Rocks

For a polymineralic rock, there is no exact formulation to calculate its bulk elastic properties (e.g., Bina & Helffrich, 1992). Averaging schemes, which distribute stress, strain, or strain energy uniformly across all grains, are provided as options in HyMaTZ. The density of the assemblage is calculated using

$$\rho = \sum V_i \rho_i \tag{6}$$

where ρ is the whole rock density and V_i and ρ_i are the volume fraction and density of each mineral constituent in the rock. For the bulk and shear moduli, Voigt's assumption (Watt et al., 1976) is that the total strain is uniform throughout the rock

$$M_v = \sum V_i M_i \tag{7}$$

where M_V is the whole-rock Voigt bulk or shear modulus and V_i and M_i are the volume fraction and bulk or shear modulus of each constituent mineral. The Reuss assumption (Watt et al., 1976) is that the stress field remains constant throughout the rock

$$\frac{1}{M_R} = \sum V_i \frac{1}{M_i} \tag{8}$$

where M_R is the whole-rock Reuss bulk or shear modulus and V_i and M_i are the volume fraction and bulk or shear modulus of each constituent mineral. A commonly used approach is to average the Voigt and Reuss bounds, which gives the Voigt-Reuss-Hill average (Watt et al., 1976)

$$M = \frac{M_R + M_v}{2} \tag{9}$$

Table 2
Experimental Data Used to Fit Regressions for the Dependence of ρ_0, K_{S0}, and G_0 on the H_2O and Fe Content of Olivine, Wadsleyite, and Ringwoodite

C_{H2O} (wt%)	X_{Fe} Fe/(Mg + Fe)	K_{S0} (GPa)	G_0 (GPa)	ρ_0 (kg/m^3)	Reference
Olivine					
0	0	129.1 (0.4)	81.6 (0.2)	3,221 (1.1)	Graham and Barsch (1969)
0	0	128.6	81.1	3,224 (0.5)	Kumazawa and Anderson (1969)
0	0	132.97 (0.07)	83.79 (0.03)	3,225	Suzuki et al. (1983)
0	0	128.8 (0.5)	81.6 (0.2)	3,225	Zha et al. (1996)
0	0.095 (0.0001)	129.37 (0.44)	78.14 (0.28)	3,353 (4)	Isaak (1992)
0	0.077 (0.0001)	131.1 (0.54)	78.95 (0.3)	3,330 (2)	Isaak (1992)
0	1 (0.01)	136.3 (0.2)	51.2 (0.2)	4,388 (9)	Speziale et al. (2004)
0	0.085	129.4	79.1	3,311	Kumazawa and Anderson (1969)
0	0.089 (0.005)	126.8	76.6	3,311	Darling et al. (2004)
0	0.099 (0.005)	127.5	78.4	3,316	Darling et al. (2004)
0	0.094 (0.005)	128.2	78.1	3,310	Darling et al. (2004)
0	0.095 (0.0001)	129.4 (0.3)	77.6 (0.3)	3,349 (3)	Webb (1989)
0	0.1 (0.0001)	129 (0.6)	77.6 (0.4)	3,362	Zaug et al. (1993)
0	0.1	131.1 (1.9)	79.4 (0.8)	3,343 (1)	Zha et al. (1998)
0	0.1	130.3 (0.4)	77.4 (0.2)	3,342 (2)	Liu et al. (2005)
0	0.11 (0.001)	129.4	78.3	3,355	Abramson et al. (1997) and Darling et al. (2004)
0.8 (0.05)	0.03	125.2 (0.8)	77.7 (0.3)	3,240 (3)	Jacobsen et al. (2008) and Jacobsen et al. (2009)
0.89 (0.05)	0	125.4 (0.2)	79.6 (0.1)	3,180 (3)	Jacobsen et al. (2008) and Mao et al. (2010)
Wadsleyite					
0	0 (0.0001)	170 (2)	115 (2)	3,488 (1)	Zha et al. (1997)
0	0	173 (1)	113 (1)	3,470 (1)	Li et al. (2001)
0	0	170.7 (1)	111.6 (1)	3,470 (1)	Li et al. (2001) and Liu et al. (2005)
0	0	170.2 (1.9)	113.9 (0.7)	3,468 (1)	Isaak et al. (2007)
0	0.08	170.8 (1.2)	108.9 (0.4)	3,581 (2)	Isaak et al. (2010)
0	0.08	170 (3)	108 (2)	3,570 (30)	Sinogeikin et al. (1998)
0	0.12 (0.001)	172 (2)	106 (1)	3,600 (4)	Li and Liebermann (2000)
0	0.13	175.4 (0.7)	108 (0.4)	3,633	Liu et al. (2009)
0.38 (0.08)	0 (0.001)	165.4 (0.9)	108.6 (0.6)	3,455 (2)	Chang et al. (2015) and Mao et al. (2008)
1.20 (0.07)	0 (0.001)	160.3 (0.7)	108.6 (0.6)	3,418 (2)	Chang et al. (2015) and Mao et al. (2008)
2.90 (0.2)	0 (0.001)	149.2 (6)	98.6 (0.4)	3,338 (2)	Chang et al. (2015) and Mao et al. (2008)
1.93 (0.22)	0.11 (0.001)	156.2 (0.5)	98 (0.3)	3,513 (1)	Mao et al. (2011)
Ringwoodite					
0	0 (0.0001)	185 (3)	120.4 (2)	3,559	Jackson et al. (2000)
0	0 (0.0001)	185 (2)	120 (1)	3,559	Li (2003)
0	0 (0.0001)	188.3 (0.3)	119.6 (0.2)	3,701 (5)	Sinogeikin et al. (2003)
0	0.09	185.1 (0.2)	118.2 (0.6)	3,700 (1)	Mayama et al. (2005)
0	0.09	186.2 (0.7)	118.5 (0.4)	3,690 (1)	Higo et al. (2008)
0	0.2	187 (2)	116 (1)	3,798 (1)	Higo et al. (2006)
0	0.25	193 (3)	113 (2)	3,878	Sinogeikin et al. (1997)
0	0.5	191 (2)	102 (1)	4,196 (1)	Higo et al. (2006)
0	1	204.5 (0.7)	73.6 (0.3)	4,846 (1)	Liu et al. (2008)
2.34	0	166.2 (0.5)	103 (5)	3,433 (1)	Wang et al. (2003) and Wang et al. (2006)
0.89	0.11	177 (4)	103.1 (0.9)	3,651 (5)	Jacobsen and Smyth (2006)
1.1 (0.06)	0.14	175.2 (1.3)	106 (1)	3,649 (3)	Mao et al. (2012)

In another averaging scheme, Hashin and Shtrikman (1963) assume that the strain energy remains constant throughout the rock, with upper bound

$$K_{HS} = K_{MAX} + \frac{V_i}{(K_i - K_{MAX})^{-1} + V_{MAX}\left(K_{MAX} - \frac{4}{3}G_{MAX}\right)^{-1}} \tag{10}$$

$$G_{HS} = G_{MAX} + \frac{V_i}{(G_i - G_{MAX})^{-1} + \frac{2V_i(K_{MAX}+2G_{MAX}}{5G_{MAX}\left(K_{MAX}+\frac{4}{3}G_{MAX}\right)}} \tag{11}$$

where K_{MAX} and G_{MAX} are the largest bulk and shear moduli among minerals in the rock and V_i, K_i, and G_i are the bulk volume fraction, bulk modulus, and shear modulus of each constituent mineral. When instead of

K_{MAX} and G_{MAX}, the lowest bulk and shear moduli among those of the minerals in the rock are used, the lower bound is obtained. The arithmetic average of the upper and lower bounds is also available as an optional averaging scheme in HyMaTZ.

2.2. Effect of Hydration on Elastic Properties

The primary function of HyMaTZ is to test the effect of H_2O on the elastic properties of $(Mg,Fe)_2SiO_4$ polymorphs (olivine, wadsleyite, and ringwoodite), viewed as seismic velocity in the MTZ. The following assumptions are made: (1) we use a planar regression to correlate between the water content, iron content, and the elasticity properties, fitted to published experimental data listed in Table 2; (2) adding a water content depth profile to HyMaTZ does not change phase equilibria of $(Mg,Fe)_2SiO_4$ polymorphs, only the density, bulk modulus, and shear modulus are affected according to the regression; and (3) pressure derivatives, $dK_{S0}/dP = K_{S0}'$ and $dG_0/dP = G_0'$, and thermal expansivity are not modified by water content unless the user specifies how they are modified by H_2O. Due to the absence of any experimental data at present, temperature derivatives of the elastic moduli are also not changed with water content.

A linear relationship is used to correlate experimental data on the effect of water and iron content on elastic properties using regression analysis in the following form:

$$M\,(X_{Fe}, C_{H2O}) = a\,(Fo_{100}, \mathrm{dry}) + b\,C_{H2O} + c\,X_{Fe} \tag{12}$$

where M represents room pressure density (ρ_0), bulk modulus (K_{S0}), or shear modulus (G_0), which are functions of mole fraction Fe content, X_{Fe} = Fe/(Fe + Mg), and water content (C_{H2O}) in weight percent (wt% H_2O per formula unit). The fitted regression parameters are a (the dry and pure Mg value of M, i.e., pure forsterite composition, Fo_{100}) and slopes b and c that give the dependence of M on water content and iron content, respectively. HyMaTZ provides two different ways to perform the regression, namely, the Sequential Least Squares Quadratic Programming and Orthogonal Distance Regression (ODR; Boggs et al., 1989) algorithms. The first (Sequential Least Squares Quadratic Programming) is meant for use when the measurement uncertainties in the dependent (response) variables are much larger than those of the independent (predictor) response variables such that the latter can be considered exact. The second (ODR) is meant for use when the relative uncertainties in both the independent and dependent variables are of the same magnitude. The use of ODR is recommended because of the lack of an absolute calibration for water content, which is an independent variable. For those studies that did not report a measurement error, we include as a default setting the average of the reported measurement errors for the same physical property and mineral; for example, the measurement error of G_0 of Kumazawa and Anderson (1969) is 0.28, which is the average of the reported measurement errors of G_0 for olivine across all studies that report an error on G_0. The user can also edit uncertainties in the experimental database for the purpose of applying a customized weighting of certain data. The experimental data are found in the file *EXPDATA*, which can be updated as new values are published in the future.

Figure 1 shows the result of the regression analysis (ODR method) performed on olivine, wadsleyite, and ringwoodite, which are also summarized in Table 2. The equations displayed on the graphs are as follows for each of the phases:

olivine:

$$\rho_0 = 3227.3(4.1) – 53.3(11.8)\,C_{H2O} + 1178.9(40.6)X_{Fe} \tag{13}$$

$$K_{S0} = 129.8(0.6) – 8.4(2.0)\,C_{H2O} + 5.9(1.8)\,X_{Fe} \tag{14}$$

$$G_0 = 81.9(0.4) – 41.8(1.2)\,C_{H2O} – 31.8(1.8)\,X_{Fe} \tag{15}$$

wadsleyite:

$$\rho_0 = 3475.3(3.3) – 48.8(3.3)\,C_{H2O} + 1179.6(48.7)X_{Fe} \tag{16}$$

$$K_{S0} = 170.4(0.7) + 8.7(0.7)\,C_{H2O} + 24.1(8.2)\,X_{Fe} \tag{17}$$

$$G_0 = 112.7(0.7) – 4.8(0.5)\,C_{H2O} – 44.0(8.7)\,X_{Fe} \tag{18}$$

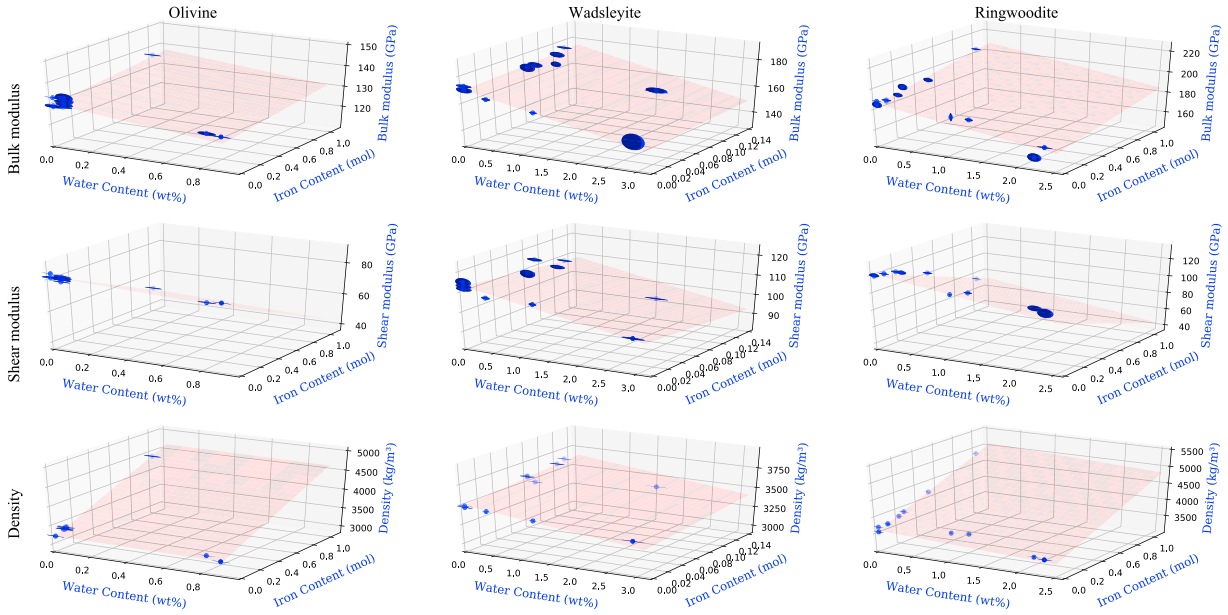

Figure 1. Regressions to published experimental data for the adiabatic bulk modulus, shear modulus, and density of $(Mg,Fe)_2SiO_4$ olivine, wadsleyite, and ringwoodite as a function of both the Fe and H_2O contents. The red plane shows the linear regression fit (ODR method). The experimental data set is presented in Table 2 and provided with HyMaTZ. The X_{Fe} scale for wadsleyite is not plotted beyond X_{Fe} = 0.15 because Fe-rich wadsleyite is not a thermodynamically stable phase.

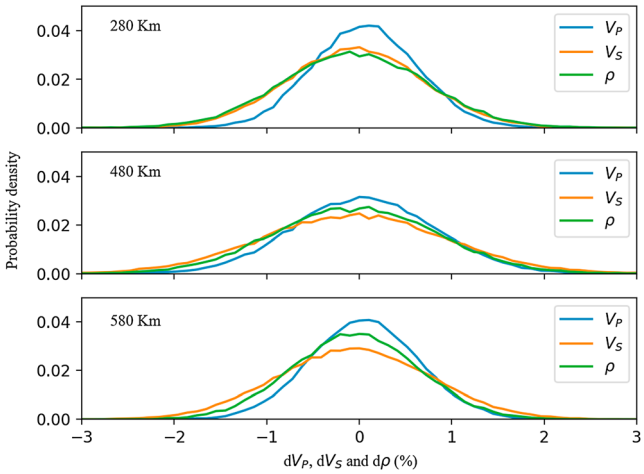

Figure 2. Distributions of the calculated seismic velocities and density due to the treating the fitted parameters of the bilinear fit (equations (13)–(21)) as random variables with a normal distribution. The error analysis used the 1600 K foot temperature and 50%WSC pyrolite model. At each depth chosen for an error analysis, 10^5 samples of the coefficients of the bilinear fit (equations (13)–(21)) were drawn to calculate the seismic velocities and density. The probability density functions do not change significantly with depth within the stability field of each olivine polymorph. As we are interested in the sensitivities to uncertainty in the coefficients, instead of using the actual but rough estimates of their uncertainty, we used 1% for the uncertainties of the a and 25% for the b and c coefficients.

ringwoodite:

$$\rho_0 = 3605.63(23.5)–98.5(20.8)\ C_{H2O} + 1209.1(58.2)\ X_{Fe} \quad (19)$$

$$K_{S0} = 186.3(1.6)–11.9(1.2)\ C_{H2O} + 12.9(2.8)\ X_{Fe} \quad (20)$$

$$G_0 = 122.8(1.9)–14.8(3.0.)\ C_{H2O}–43.6(3.1)\ X_{Fe} \quad (21)$$

In equations (13)–(21), the numbers in parentheses are 1σ uncertainties in the corresponding coefficients. Some of the uncertainties in the fitted coefficients shown in equations (13)–(21) are large. This is due to the fact that there are few data points along with scatter in the data. We conducted error analysis with the Monte Carlo (statistical) method (Connolly & Khan, 2016), showing that the propagated errors in seismic velocities are less than 1% (Figure 2). The reason for this is because the physical properties were mainly determined by the *a* coefficient (constant term) in the correlation, and the uncertainty for that is small. Conversely, the large uncertainties in the *b* coefficients, which is the slope along the water concentration axis, indicate that there would be a large uncertainty when variations in the seismic velocity are used to estimate the water concentration by inversion. The error analysis results shown in Figure 2 give the distributions in the seismic velocities and density when the coefficients in equations (13)–(21) are treated as random variables with a normal distribution. The calculation used the 1600 K foot temperature and 50% water storage capacities (WSC) pyrolite model.

2.3. Water Content Depth Profiles

Olivine, wadsleyite, and ringwoodite have different WSC, which is the maximum water content in the solid phase without stabilizing a coexisting hydrous melt or fluid (Hirschmann et al., 2005). The water storage capacity of $(Mg,Fe)_2SiO_4$ polymorphs varies with pressure, temperature, oxygen fugacity, and bulk (rock) mineral assemblage (e.g., Bolfan-Casanova et al.,

2012; Demouchy et al., 2005; Kohlstedt et al., 1996; Tenner et al., 2012). For simplicity, HyMaTZ works with a user-defined water content profile, which refers to variation in the amount of water in the $(Mg,Fe)_2SiO_4$ phases as a function of depth. To create the default water content depth profile, we take storage capacity for wadsleyite to be 3.3 wt% (Smyth, 1987) and then apply partition coefficients of 6:30:15 for the ratios of water in olivine: wadsleyite: ringwoodite from Inoue et al. (2010). The water content profile of olivine as a function of depth was taken from the experimental data of Hauri et al. (2006). To produce different water content profiles through the upper mantle and transition zone, the user specifies the percentage of storage capacity for each phase. For example, if the user specifies 50% WSC for their profile, wadsleyite will have 1.65 wt% H_2O (constant) and ringwoodite will have half that or 0.825 wt% H_2O (constant). The partition coefficient between olivine: wadsleyite from Inoue et al., 2010 is 6:30, so in the above example (50% WSC), the olivine at 410-km depth would have 5 times less water than the wadsleyite or 0.33 wt% H_2O. The variation of water in olivine with depth still follows the depth profile given in Hauri et al. (2006), but it is anchored to 0.33 wt% H_2O at 410-km depth. We note that the partitioning of water between wadsleyite and olivine here is a simplistic approach and does not account for partitioning of water between olivine and the full pyrolitic assemblage (Tenner et al., 2012) nor can it account for the production of partial melting when the storage capacity of one phase is exceeded across the phase boundaries. HyMaTZ also allows the user to provide a custom water content profile by specifying in equation form how the water content varies with depth for each phase of $(Mg,Fe)_2SiO_4$. If the user does not select to modify elastic properties with hydration from the regression fittings, rather than using the dry density and elastic moduli obtained from the regression, the thermoelastic properties from the Perple_X output will be applied.

2.4. Anelasticity

The velocities calculated by equations (1) and (2) neglect the effect of internal friction and hence are independent of frequency. However, it is known that some velocity dispersion and attenuation of seismic waves occur, and theoretical calculations and experimental work (Karato, 1993; Karato & Spetzler, 1990) have shown that the underlying anelasticity can also decrease seismic velocities. Karato and Jung (1998) showed that water can significantly reduce seismic wave velocities through anelastic effects. In HyMaTZ, one has the option to correct the calculated mineral acoustic velocities with anelasticity models derived from long-period seismic data analysis by the following equations (Goes et al., 2000; Minster & Anderson, 1981):

$$Q_s = Q_\mu = A\omega \exp\left(\frac{aH}{RT}\right) \tag{22}$$

$$H = E + PV \tag{23}$$

$$Q_P^{-1} = (1 - L)Q_k^{-1} + LQ_\mu^{-1} \tag{24}$$

$$L = \left(\frac{4}{3}\right) * \left(\frac{V_s}{V_P}\right) \tag{25}$$

$$V_{(P,T,X,\omega)} = V_{(P,T,X)}\left(1 - \frac{Q^{-1}(\omega, T)}{2\tan\left(\frac{\pi a}{2}\right)}\right) \tag{26}$$

where A is a constant, R is the gas constant, H is activation enthalpy, and E is activation energy, and equation (22) is based on a thermodynamic (transition state theory) correlation of relaxation times versus temperature and pressure. V is activation volume, ω is the seismic frequency, a is the frequency exponent in the power law model of Q and $0 \leq a \leq 1$, and P and T are pressure and temperature. Q_S and Q_P are the Q values for P and S waves, and Q_μ and Q_K are the Q values for the bulk and shear moduli. In the mantle, $Q_K >> Q_S$ and is usually taken to be infinity. HyMaTZ also contains attenuation models by Cammarano et al. (2003) and Goes et al. (2000). The user can also input a custom attenuation model.

3. Results

3.1. Benchmarking

Running HyMaTZ consists of several steps: (1) selecting a compositional model, (2) calculating phase proportions along a user-selected adiabatic temperature gradient, (3) applying a water content profile,

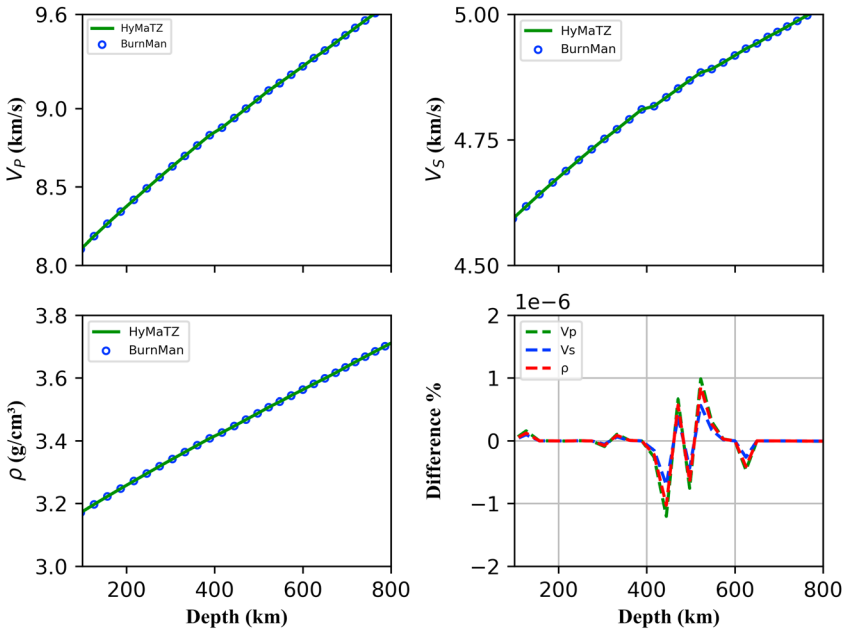

Figure 3. Comparison of output from HyMaTZ (green curves) and BurnMan (blue open circles; Cottaar et al., 2014) for V_P, V_S, and density of pure forsterite along a 1600-K adiabatic temperature gradient. HyMaTZ = Hydrous Mantle Transition Zone.

(4) choosing how water influences thermoelastic properties of olivine polymorphs, and finally (5) selecting a polycrystalline averaging scheme. To test the validity of our approach against previous work, we provide comparisons to some existing programs for the case of a dry MTZ. Figure 3 shows a comparison of HyMaTZ output with the output from the BurnMan code (Cottaar et al., 2014) for pure forsterite,

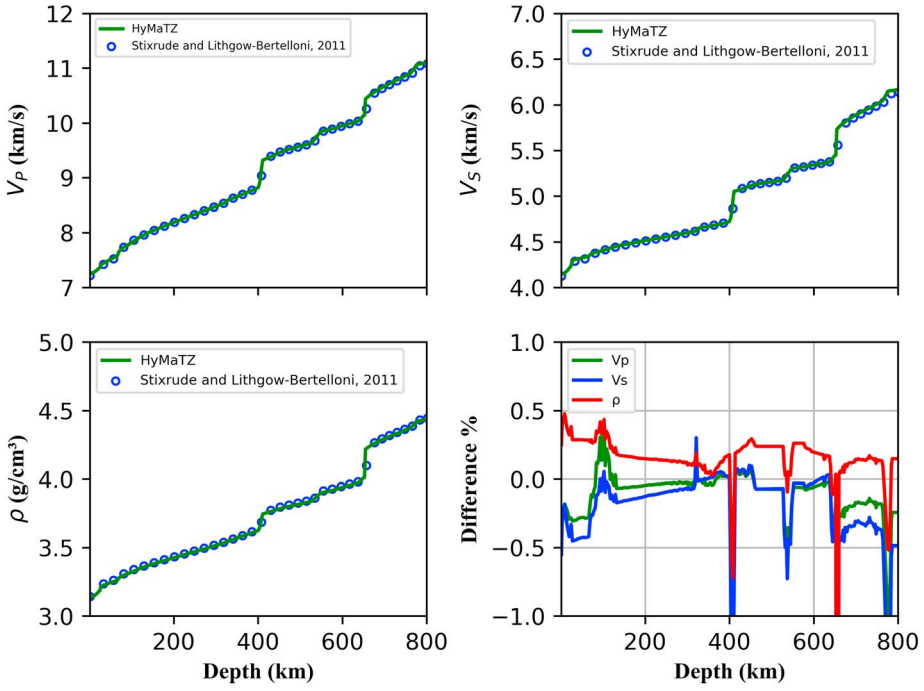

Figure 4. Comparison of velocities obtained for the 1600-K isentropic pyrolite model from HyMaTZ with those computed by Stixrude and Lithgow-Bertelloni (2011). HyMaTZ = Hydrous Mantle Transition Zone.

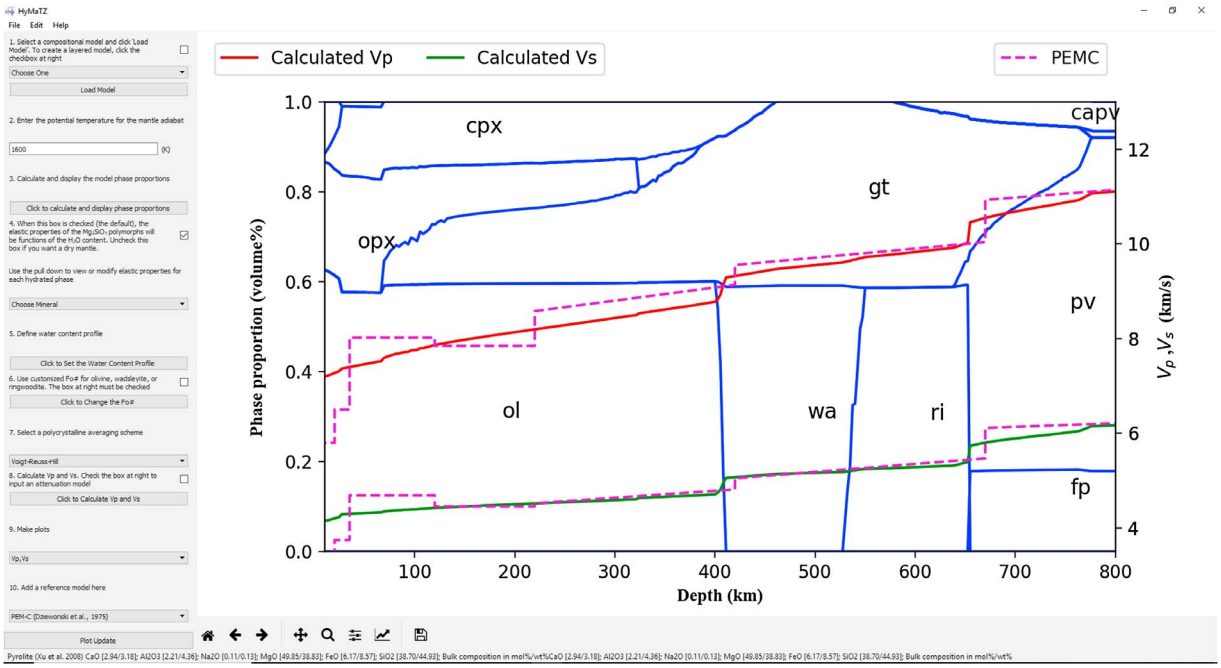

Figure 5. Screenshot of the HyMaTZ dashboard. A set of instructions appear along the left-hand side of the dashboard. At right, the phase proportions and velocities are plotted, along with a comparison to the PEMC model (Dziewonski et al., 1975). HyMaTZ = Hydrous Mantle Transition Zone.

Mg_2SiO_4. At all conditions between 200- and 800-km depth, the difference between HyMaTZ and Burnman velocities for Mg_2SiO_4 is less than 5×10^{-6}%.

Next we compare the output of HyMaTZ to predicted seismic velocities from Perple_X using the database of Stixrude and Lithgow-Bertelloni (2011). Because HyMaTZ uses the same EOS in Perple_X, this benchmark tests our usage of the implementation of the EOS. Figure 4 shows a typical comparison with data provided by Stixrude and Lithgow-Bertelloni (2011) for a 1600-K isentropic pyrolite model. We observe a difference of up to ±0.5% in V_P and V_S, mainly at the major phase transition depths (410, 520, and 660 km), which may be due to two reasons. First, although Perple_X produced phase proportions very close to those of Stixrude and Lithgow-Bertelloni (2011), there were still some small differences in phase proportions that can lead to 0.5% difference in the seismic velocities and densities. This difference is possibly because we calculate phase proportions on a 2-D grid and then use interpolation to obtain parameters in between grid points; thus, the phase proportions are not exactly the same as the directly calculated values when the pressure and temperature are not on a grid point. Second, we calculated the pressure and temperature versus depth profiles using the interpolated phase proportions; thus, the differences in the phase proportions will propagate to the calculated pressures and temperatures. This was most obvious in the region of the seismic discontinuities, that is, the largest differences of up to 1% between HyMaTZ velocities and those of Stixrude and Lithgow-Bertelloni (2011) were around the 410-, 660-, and 730-km phase boundaries. A slight difference in the *P-T* node conditions can cause a small shift in the depth of the phase transition. Overall, HyMaTZ produces velocity profiles for dry pyrolite that are broadly consistent with Burnman and Perple_X using the Stixrude and Lithgow-Bertelloni (2011) database.

3.2. A Sample Calculation

As an example of how the program is run, we go through a HyMaTZ calculation using the pyrolite model (Xu et al., 2008) for a 1600-K adiabatic temperature profile. Detailed instructions are provided in the downloadable software manual. Figure 5 shows the HyMaTZ dashboard. Along the left-hand side of the dashboard, HyMaTZ displays a numbered list of instructions that are followed stepwise: (1) select a compositional model, (2) set the adiabatic foot temperature at the surface, (3) display the phase proportion model, (4) indicate whether a dry or hydrous model will be used for $(Mg,Fe)_2SiO_4$ phases, and (5) define the water content profile. In step 6, the user can alter the forsterite number (Fo#) of $(Mg,Fe)_2SiO_4$ polymorphs, in which case the values

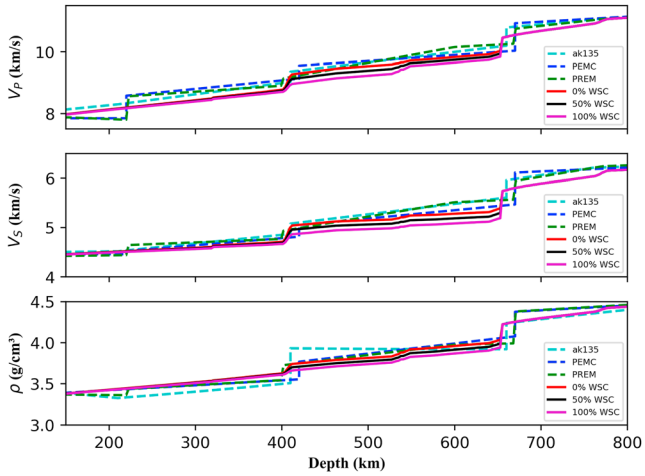

Figure 6. The effect of water content (WSC: water storage capacity) in the $(Mg,Fe)_2SiO_4$ polymorphs on the seismic velocities and density compared with some 1-D global models. The calculations here used a 1600-K isentropic temperature profile and a mantle of pyrolite composition (Xu et al., 2008).

of density, K_{S0}, and G, are derived from the fitted regressions in step 4. However, if the user customizes the Fo# in the olivine polymorphs, it should be clarified that there will be no effect on the phase proportions, which were fixed in step 1. Instead, this variable is only meant to allow one to test the comparative effects of changing Fe and H_2O on velocities. In step 7, a polycrystalline averaging scheme is selected, and in step 8 the user can select an attenuation model, if desired. In step 9, the velocities are calculated, and in step 10 the user can select what to plot, such as V_P, V_S, V_P/V_S, temperature, bulk modulus, shear modulus, or density. In step 11, one can add a reference model for comparison, including PREM (Dziewonski et al., 1975), ak135 (Kennett et al., 1995), IASP91 (Kennett & Engdahl, 1991), or PEM-C (Dziewonski et al., 1975). In addition, the user can input a custom velocity profile here, which, for example, could be a user-generated regional velocity model.

Figure 6 further illustrates how the results of a velocity calculation are displayed. In this example we calculate velocities through a pyrolite model (Xu et al., 2008) with a 1600-K adiabatic foot temperature. The results of a dry (0% WSC) and two hydrous models are displayed, where 50% WSC indicates 50% of maximum water storage capacity, being 1.5 wt% H_2O for wadsleyite and partitioned according to Inoue et al. (2010)) and 100% WSC representing full water storage capacity (i.e., 3.3 wt% H_2O in wadsleyite). For comparison, we plot several global 1-D models, ak135 (Kennett et al., 1995), PEMC (Dziewonski et al., 1975), and PREM (Dziewonski & Anderson, 1981). In this example, a dry transition zone is most consistent with global 1-D models. HyMaTZ can also be used as a research tool to evaluate regional seismic velocity models. Such an example is given in section 3.4.

3.3. Trade-Offs in Parameters Influencing Seismic Velocity

Temperature is the most sensitive parameter in calculating seismic velocities because it strongly influences both phase proportions and thermoelastic variables. Several studies have focused on how the temperature affects seismic velocities (Goes et al., 2000; Goes & Van der Lee, 2002), suggesting that just 100-K difference could influence V_S by ~1% in the shallow mantle and by 0.5% in the lower transition zone (Cammarano et al., 2003). Composition is another sensitive factor in the calculation of seismic velocities. Cammarano et al. (2003) performed calculations with varied Fe, Al, and Ca contents and found that an increase in the Fe content from 7% to 11% gave decreased V_S by 1% and V_P by 0.7%. Xu et al. (2008) suggested that the mantle may be heterogeneous, being better represented by a mechanical mixture of basalt and harzburgite, and they showed that the V_S in a mechanical-mixture transition zone is faster and increases more rapidly with depth. Accordingly, in HyMaTZ, we provide several options that let the user examine how mechanical mixtures of compositional models change the calculated seismic velocity profiles. Figure 7 shows an example of how temperature, water, and Fe content trade off in the calculated velocity profile of pyrolite in the transition zone. Compared with a dry MTZ, increasing the water content in wadsleyite to 1.65 wt% (50% WSC), increasing the temperature by 160 K, or increasing the Fe content from Fo_{90} to Fo_{83} (increase of X_{Fe} = 0.07) produce comparable reductions in seismic velocity for the pyrolite model.

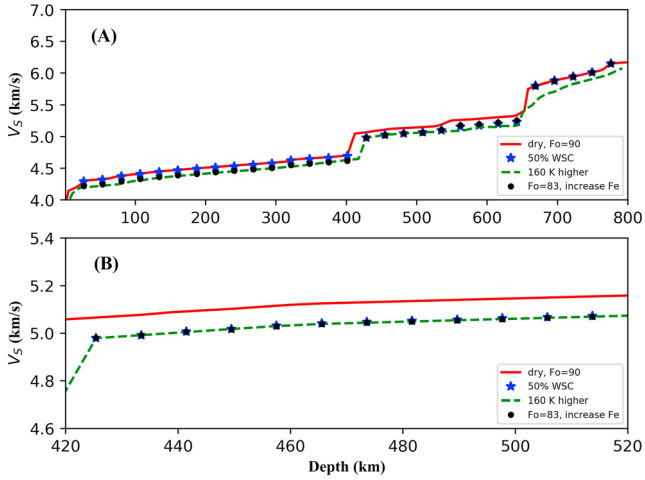

Figure 7. (a) A comparison of *S* wave velocity for a 1600 K dry pyrolite model (solid red line) with adding 50% water storage capacity to $(Mg,Fe)_2SiO_4$ polymorphs (blue stars), increasing the temperature of a dry pyrolite model by 160 K (green dashed curve), and adding 7 mol% of Fe to a 1600 K dry pyrolite (black circles). (b) Expanded view showing only the upper transition zone (410–520 km), where these parameters were adjusted to produce equivalent velocity profiles. WSC = water storage capacities.

Whereas HyMaTZ modifies ρ, K_S, and G with hydration through a regression to experimental data, the pressure derivatives of these parameters are taken to be unchanged from those in the thermodynamic database, parameterized according to the Birch-Murnaghan EOS. However, the user can also input customized pressure derivatives to test the influence of

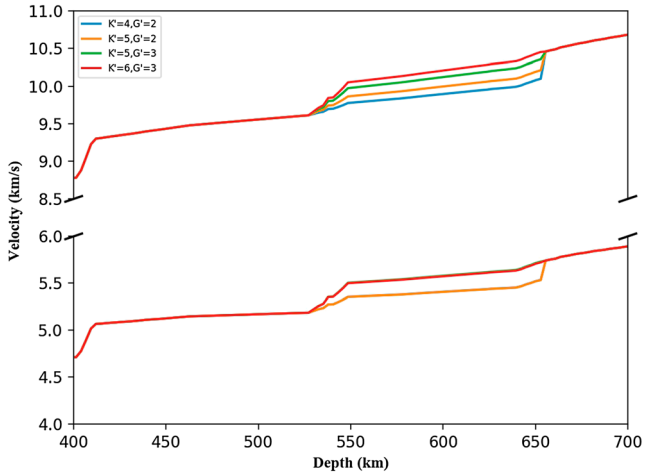

Figure 8. *P* and *S* wave velocities of 1600 K dry pyrolite in the transition zone shown for varying values of K_0' and G_0' in ringwoodite.

$K_0 = (\mathrm{d}K/\mathrm{d}P)_{P=0}$ and $G_0' = (\mathrm{d}G/\mathrm{d}P)_{P=0}$. In Figure 8, the outcome for several combinations of K_0' and G_0' is plotted, which may be influenced by water content. For example, whereas Chang et al. (2015) show that water does not strongly influence K_0' of wadsleyite, elasticity data for hydrous ringwoodite suggest elevated K_0' and G_0' (Jacobsen & Smyth, 2006; Smyth et al., 2004; Thio et al., 2016; Wang et al., 2006; Ye et al., 2012). In Figure 8, velocities of dry pyrolite are shown when the K_0' and G_0' of ringwoodite are varied to illustrate the influence of the pressure derivatives.

3.4. Influence of Water on the Seismic Velocity in the Transition Zone: Comparison With a Regional Model

Van der Lee and Nolet (1997) used regional waveform tomography to image mantle structure beneath the North American continent. Their results showed that in the MTZ beneath the eastern U.S. continental margin shear wave velocities reach to over 1% lower than the continental average, confirming earlier hints for such a deep low-velocity region (Grand, 1994; Romanowicz, 1979). Van der Lee et al. (2008) showed that in 3-D tomographic model NA04 of Van der Lee and Frederiksen (2005), the East Coast anomaly extends from transition zone depths up to depths around 100 km beneath the U.S. East Coast. The anomaly is also present in more recent tomographic models such as NA07 (Bedle & Van der Lee, 2009) and SL2013NA (Schaeffer & Lebedev, 2014) which includes USArray data. Van der Lee et al. (2008) argued that a changed temperature profile is not an obvious explanation for the anomaly because there is neither an obvious heat source (such as a mantle plume) in tomographic models nor do independent observations of discontinuity characteristics or surface heat flow suggest elevated heat (Goes & Van der Lee, 2002; Pollack et al., 1993). At least one study shows evidence for an uplifted 410-km discontinuity and a strengthened 520-km discontinuity beneath the eastern United States (Courtier & Revenaugh, 2006), suggesting that hydration of the upper mantle provides an alternative explanation.

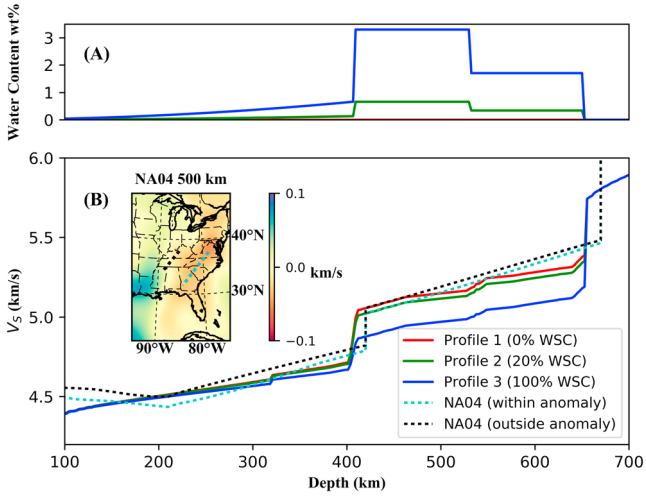

Figure 9. (a) Three water content profiles in $(Mg,Fe)_2SiO_4$ phases of a pyrolite model used to show the effect of waters: blue, maximum water; green, intermediate water; and red, dry pyrolite. The profiles are created by adding 3.3 wt% H_2O to wadsleyite in the maximum water model (100% WSC) and then partitioning water at 410 and 520 km based on the partition coefficients from Inoue et al. (2010). Thus, the blue curve represents 0.66, 3.3, and 1.7 wt% H_2O in olivine (at 410 km), wadsleyite, and ringwoodite, respectively, while the green curve (20% WSC) represents 0.13, 0.66, and 0.33 wt% H_2O in olivine (at 410 km), wadsleyite, and ringwoodite, respectively. (b) *S* wave velocity profiles for these different water content depth profiles compared with the 1-D average velocity profile representing the eastern U.S. low-velocity anomaly in the NA04 model (turquoise dashed line). For comparison, the black dashed line shows a 1-D average velocity profile from just outside the eastern U.S. low-velocity anomaly. Geographic location of the profiles within (turquoise dashed line) and outside the anomaly (black dashed line) is shown on the 500-km depth tomographic image, inset, from Van der Lee and Frederiksen (2005).

We used three different water content depth profiles that simulate a dry mantle, a hypothesized intermediate mantle condition, and a maximally wet mantle, and we synthesized their velocity profiles, illustrated in Figure 9. Profile 1 (red line) is for the case of a dry mantle. Profile 2 (green line) is constructed for 20% WSC (i.e., 0.13 wt% H_2O in olivine at 410 km, 0.65 wt% H_2O in wadsleyite, and 0.33 wt% H_2O in ringwoodite). Profile 3 (blue line) is for the case where the WSC is maximum (i.e., 0.66 wt% H_2O in olivine at 410 km, 3.3 wt% H_2O in wadsleyite, and 1.7 wt% H_2O in ringwoodite). Two regional *S* wave velocity profiles were constructed as the 1-D average through a portion of 3-D model NA04 (Van der Lee & Frederiksen, 2005), of which one averages the eastern U.S. low-velocity anomaly region and one represents an average from outside the anomaly region. For all three water content profiles, calculated velocities in the uppermost mantle are similar to or lower than the reference seismic profile from outside the anomaly. The three profiles are similar to the seismic profile from within the low-velocity anomaly between 280 and 340 km, but their gradients are less steep than the seismic profile's gradient.

While hydration could affect the velocities in NA04 at depths shallower than 400 km, uncertainties in the velocity gradient of the seismic reference model preclude an unambiguous interpretation of the absolute velocities. The transition zone exhibits more variations in the HyMaTZ profiles as a result of hydration. Figure 9 suggests that the uppermost part of the transition zone beneath eastern North America may be moderately hydrous,

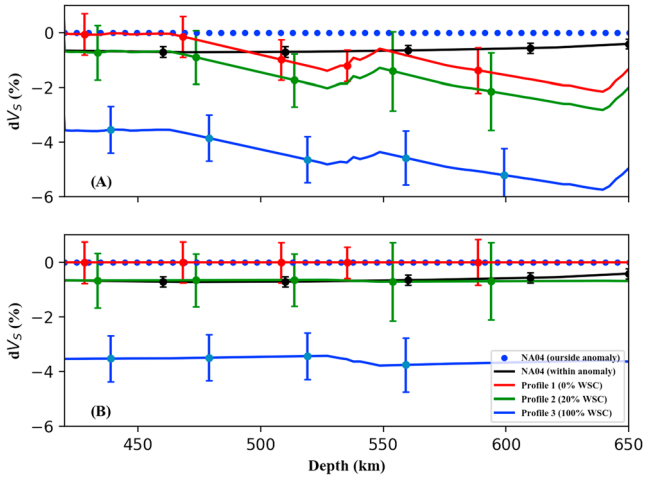

Figure 10. The same velocity profiles as shown in Figure 9 but relative to the reference seismic velocity profile (a). (b) The same anomalous seismic velocity profile as (a) but the calculated water content profiles are relative to the reference mineralogical model (dry pyrolite, red curve in a and Figure 9b). The difference shows how water can change the velocity relative to a dry pyrolite model. The three water content profiles in $(Mg,Fe)_2SiO_4$ phases of a pyrolite model show the effect of water: blue, maximum water; green, intermediate water; and red, dry pyrolite.

since the dry model (red curve) matches velocities outside the eastern U.S. low-velocity region and the model constructed with 20% water storage capacity (green curve) compares well to the 1-D average profile within the eastern U.S. low-velocity anomaly, as previously suggested by Van der Lee et al. (2008). However, comparison of absolute velocities across the entire depth region of the MTZ shows significant differences between the HyMaTZ calculations and the velocities from seismic models, mostly, and as above, as a result of the HyMaTZ reference velocity model having a less steep gradient than the reference seismic profile's gradient. Removing the seismic reference velocities from the anomalous velocities and removing the dry HyMaTZ velocities from the other HyMaTZ velocity profiles allow us to compare velocity anomalies (Figure 10b). Figure 10a shows the differences of the profiles in Figure 9b with respect to the reference seismic model (black dotted line), which allows us to visualize error bars reflecting uncertainties in the HyMaTZ profiles estimated above and uncertainties in the seismic profiles estimated by Bedle and Van der Lee (2009) from an ensemble of tomographic models with good data fits. These tomographic models are guided to depart minimally from a reference model and also have a limited range of smoothness constraints, likely leaving the uncertainties underestimated. Figure 10b shows that the green water content profile fits the seismic profile for the anomaly well, within uncertainties, over the entire depth range of the transition zone, suggesting that a mantle with olivine polymorph water content of 20% of the storage capacity is a reasonable explanation for the anomaly.

The differences in seismic velocity gradients between velocity profiles derived from seismic data and velocity profiles calculated by HyMaTZ require further interpretation. For example, in the lower part of the transition zone, all HyMaTZ model calculations (including the dry one) are slower than seismically modeled velocities. This may be reconciled by increasing the pressure derivative of the shear modulus of ringwoodite (consistent with hydration), by decreasing or varying the MTZ velocity gradient in the seismic reference model used in the tomography, or by changing the mineralogical model in the lower part of the MTZ (Anderson & Bass, 1986; Weidner, 1986).

4. Conclusions

1. HyMaTZ is a freely available Python code with graphical user interface used to calculate seismic velocity profiles for various mineralogical models where the elastic properties of $(Mg,Fe)_2SiO_4$ polymorphs may be varied by effects due to hydration, calculated from a regression of experimental data.
2. At conditions of the uppermost transition zone, increasing the water content in wadsleyite to 1.65 wt% H_2O (50% WSC) causes an equivalent reduction in *S* wave velocity in pyrolite as increasing the iron content by 7 mol% or raising the temperature of a 1600-K pyrolite model by 160 K.
3. The eastern U.S. low-velocity anomaly is consistent with wadsleyite and ringwoodite in pyrolite containing 0.65 and 0.33 wt% H_2O (20% WSC), respectively, but the absolute velocity of the lower MTZ is faster than all HyMaTZ models, suggesting that the pressure derivatives of ringwoodite should be elevated (consistent with hydration), the seismic-velocity gradient should be reduced and/or vary with depth in the seismic model, or an alternative compositional model is required to better fit the deeper MTZ.

Acknowledgments
This research was supported by the National Science Foundation grant EAR-1452344 to S. D. J. HyMaTZ can be downloaded from GitHub at github.com/wangyefei/HyMaTZ. HyMaTZ can be redistributed and/or modified under the terms of the GNU Library General Public License as published by the Free Software Foundation. All of the data sets used in this paper are provided in the software distribution.

References

Abramson, E. H., Brown, J. M., Slutsky, L. J., & Zaug, J. M. (1997). The elastic constants of San Carlos olivine to 17 GPa. *Journal of Geophysical Research*, *102*(B6), 12,253–12,263. https://doi.org/10.1029/97JB00682

Afonso, J. C., Fernandez, M., Ranalli, G., Griffin, W. L., & Connolly, J. A. D. (2008). Integrated geophysical-petrological modeling of the lithosphere and sublithospheric upper mantle: Methodology and applications. *Geochemistry, Geophysics, Geosystems*, *9*, Q05008. https://doi.org/10.1029/2007GC001834

Anderson, D. L., & Bass, J. D. (1986). Transition region of the Earth's uppper mantle. *Nature*, *320*(6060), 321–328. https://doi.org/10.1038/320321a0

Barklage, M., Wiens, D. A., Conder, J. A., Pozgay, S., Shiobara, H., & Sugioka, H. (2015). *P* and *S* velocity tomography of the Mariana subduction system from a combined land-sea seismic deployment. *Geochemistry, Geophysics, Geosystems*, *16*, 681–704. https://doi.org/10.1002/2014GC005627

Bedle, H., & Van der Lee, S. (2009). *S* velocity variations beneath North America. *Journal of Geophysical Research*, *114*, B07308. https://doi.org/10.1029/2008JB005949

Bina, C. R., & Helffrich, G. R. (1992). Calculation of elastic properties from thermodynamic equation of state principles. *Annual Review of Earth and Planetary Sciences*, *20*(1), 527–552. https://doi.org/10.1146/annurev.ea.20.050192.002523

Boggs, P. T., Donaldson, J. R., Byrd, R. H., & Schnabel, R. B. (1989). Algorithm 676 ODRPACK: Software for weighted orthogonal distance regression. *ACM Transactions on Mathematical Software*, *15*(4), 348–364. https://doi.org/10.1145/76909.76913

Bolfan-Casanova, N. (2005). Water in the Earth's mantle. *Mineralogical Magazine*, *69*(03), 229–257. https://doi.org/10.1180/0026461056930248

Bolfan-Casanova, N., Muñoz, M., McCammon, C., Deloule, E., Férot, A., Demouchy, S., et al. (2012). Ferric iron and water incorporation in wadsleyite under hydrous and oxidizing conditions: A XANES, Mössbauer, and SIMS study. *American Mineralogist*, *97*(8–9), 1483–1493. https://doi.org/10.2138/am.2012.3869

Burdick, S., Vernon, F. L., Martynov, V., Eakins, J., Cox, T., Tytell, J., et al. (2017). Model update May 2016: Upper-mantle heterogeneity beneath North America from travel-time tomography with global and USArray data. *Seismological Research Letters*, *88*(2A), 319–325. https://doi.org/10.1785/0220160186

Cammarano, F., Goes, S., Vacher, P., & Giardini, D. (2003). Inferring upper-mantle temperatures from seismic velocities. *Physics of the Earth and Planetary Interiors*, *138*(3–4), 197–222. https://doi.org/10.1016/S0031-9201(03)00156-0

Chang, Y.-Y., Jacobsen, S. D., Bina, C. R., Thomas, S.-M., Smyth, J. R., Frost, D. J., et al. (2015). Comparative compressibility of hydrous wadsleyite and ringwoodite: Effect of H_2O and implications for detecting water in the transition zone. *Journal of Geophysical Research: Solid Earth*, *120*, 8259–8280. https://doi.org/10.1002/2015JB012123

Chen, J. h., Inoue, T., Yurimoto, H., & Weidner, D. J. (2002). Effect of water on olivine-wadsleyite phase boundary in the (Mg, Fe) $_2SiO_4$ system. *Geophysical Research Letters*, *29*(18), 1875. https://doi.org/10.1029/2001GL014429

Connolly, J. A. D. (2005). Computation of phase equilibria by linear programming: A tool for geodynamic modeling and its application to subduction zone decarbonation. *Earth and Planetary Science Letters*, *236*(1–2), 524–541. https://doi.org/10.1016/j.epsl.2005.04.033

Connolly, J. A. D. (2009). The geodynamic equation of state: What and how. *Geochemistry, Geophysics, Geosystems*, *10*, Q10014. https://doi.org/10.1029/2009GC002540

Connolly, J. A. D., & Khan, A. (2016). Uncertainty of mantle geophysical properties computed from phase equilibrium models. *Geophysical Research Letters*, *43*, 5026–5034. https://doi.org/10.1002/2016GL068239

Cottaar, S., Heister, T., Rose, I., & Unterborn, C. (2014). BurnMan: A lower mantle mineral physics toolkit. *Geochemistry, Geophysics, Geosystems*, *15*, 1164–1179. https://doi.org/10.1002/2013GC005122

Courtier, A. M., & Revenaugh, J. (2006). A water-rich transition zone beneath the eastern United States and Gulf of Mexico from multiple ScS reverberations. In S. D. Jacobsen, & S. Van der Lee (Eds.), *Earth's deep water cycle* (pp. 181–193). Washington DC: American Geophysical Union.

Darling, K. L., Gwanmesia, G. D., Kung, J., Li, B. S., & Liebermann, R. C. (2004). Ultrasonic measurements of the sound velocities in polycrystalline San Carlos olivine in multi-anvil, high-pressure apparatus. *Physics of the Earth and Planetary Interiors*, *143*, 19–31.

Demouchy, S., Deloule, E., Frost, D. J., & Keppler, H. (2005). Pressure and temperature-dependence of water solubility in Fe-free wadsleyite. *American Mineralogist*, *90*(7), 1084–1091.

Dziewonski, A. M., & Anderson, D. L. (1981). Preliminary reference Earth model. *Physics of the Earth and Planetary Interiors*, *25*(4), 297–356. https://doi.org/10.2138/am.2005.1751

Dziewonski, A. M., Hales, A. L., & Lapwood, E. R. (1975). Parametrically simple Earth models consistent with geophysical data. *Physics of the Earth and Planetary Interiors*, *10*(1), 12–48. https://doi.org/10.1016/0031-9201(75)90017-5

Emry, E. L., Nyblade, A. A., Julia, J., Anandakrishnan, S., Aster, R. C., Wiens, D. A., et al. (2015). The mantle transition zone beneath West Antarctica: Seismic evidence for hydration and thermal upwellings. *Geochemistry, Geophysics, Geosystems*, *16*, 40–58. https://doi.org/10.1002/2014GC005588

Fei, H. Z., Yamazaki, D., Sakurai, M., Miyajima, N., Ohfuji, H., Katsura, T., & Yamamoto, T. (2017). A nearly water-saturated mantle transition zone inferred from mineral viscosity. *Science Advances*, *3*(6), e1603024. https://doi.org/10.1126/sciadv.1603024

French, S. W., & Romanowicz, B. A. (2014). Whole-mantle radially anisotropic shear velocity structure from spectral-element waveform tomography. *Geophysical Journal International*, *199*(3), 1303–1327. https://doi.org/10.1093/gji/ggu334

Frost, D. J. (2006). The stability of hydrous mantle phases. *Reviews in Mineralogy and Geochemistry*, *62*(1), 243–271. https://doi.org/10.2138/rmg.2006.62.11

Frost, D. J., & Dolejš, D. (2007). Experimental determination of the effect of H_2O on the 410-km seismic discontinuity. *Earth and Planetary Science Letters*, *256*(1-2), 182–195. https://doi.org/10.1016/j.epsl.2007.01.023

Goes, S., Govers, R., & Vacher, P. (2000). Shallow mantle temperatures under Europe from *P* and *S* wave tomography. *Journal of Geophysical Research*, *105*(B5), 11,153–11,169. https://doi.org/10.1029/1999JB900300

Goes, S., & Van der Lee, S. (2002). Thermal structure of the North American uppermost mantle inferred from seismic tomography. *Journal of Geophysical Research*, *107*(B3), 2050. https://doi.org/10.1029/2000JB000049

Graham, E. K., & Barsch, G. R. (1969). Elastic constants of single-crystal forsterite as a function of temperature and pressure. *Journal of Geophysical Research*, *74*(25), 5949–5960. https://doi.org/10.1029/JB074i025p05949

Grand, S. P. (1994). Mantle shear structure beneath the Americas and surrounding oceans. *Journal of Geophysical Research*, *99*(B6), 11,591–11,621. https://doi.org/10.1029/94JB00042

Grand, S. P. (2002). Mantle shear-wave tomography and the fate of subducted slabs. *Philosophical Transactions of the Royal Society A*, *360*(1800), 2475–2491. https://doi.org/10.1098/rsta.2002.1077

Green, H. W., Chen, W. P., & Brudzinski, M. R. (2010). Seismic evidence of negligible water carried below 400-km depth in subducting lithosphere. *Nature*, *467*(7317), 828–831. https://doi.org/10.1038/nature09401

Hashin, Z., & Shtrikman, S. (1963). A variational approach to the theory of the elastic behaviour of multiphase materials. *Journal of the Mechanics and Physics of Solids*, *11*(2), 127–140. https://doi.org/10.1016/0022-5096(63)90060-7

Hauri, E. H., Gaetani, G. A., & Green, T. H. (2006). Partitioning of water during melting of the Earth's upper mantle at H_2O-undersaturated conditions. *Earth and Planetary Science Letters*, *248*(3-4), 715–734. https://doi.org/10.1016/j.epsl.2006.06.014

Higo, Y., Inoue, T., Irifune, T., Funakoshi, K. I., & Li, B. S. (2008). Elastic wave velocities of $(Mg_{0.91}Fe_{0.09})_2SiO_4$ ringwoodite under P-T conditions of the mantle transition region. *Physics of the Earth and Planetary Interiors*, *166*(3-4), 167–174. https://doi.org/10.1016/j.pepi.2008.01.003

Higo, Y., Inoue, T., Li, B. S., Irifune, T., & Liebermann, R. C. (2006). The effect of iron on the elastic properties of ringwoodite at high pressure. *Physics of the Earth and Planetary Interiors*, *159*(3–4), 276–285. https://doi.org/10.1016/j.pepi.2006.08.004

Hirschmann, M. M. (2006). Water, melting, and the deep Earth H_2O cycle. *Annual Review of Earth and Planetary Sciences*, *34*(1), 629–653. https://doi.org/10.1146/annurev.earth.34.031405.125211

Hirschmann, M. M., Aubaud, C., & Withers, A. C. (2005). Storage capacity of H_2O in nominally anhydrous minerals in the upper mantle. *Earth and Planetary Science Letters*, *236*(1-2), 167–181. https://doi.org/10.1016/j.epsl.2005.04.022

Holland, T. J. B., Hudson, N. F. C., Powell, R., & Harte, B. (2013). New thermodynamic models and calculated phase equilibria in NCFMAS for basic and ultrabasic compositions through the transition zone into the uppermost lower mantle. *Journal of Petrology*, *54*(9), 1901–1920. https://doi.org/10.1093/petrology/egt035

Inoue, T., Wada, T., Sasaki, R., & Yurimoto, H. (2010). Water partitioning in the Earth's mantle. *Physics of the Earth and Planetary Interiors*, *183*(1–2), 245–251. https://doi.org/10.1016/j.pepi.2010.08.003

Irifune, T., & Ringwood, A. E. (1987). Phase-transformations in a Harzburgite composition to 26 Gpa—Implications for dynamical behavior of the subducting slab. *Earth and Planetary Science Letters*, *86*(2–4), 365–376. https://doi.org/10.1016/0012-821X(87)90233-0

Isaak, D. G. (1992). High-temperature elasticity of iron-bearing olivines. *Journal of Geophysical Research*, *97*(B2), 1871–1885. https://doi.org/10.1029/91JB02675

Isaak, D. G., Gwanmesia, G. D., Davis, M. G., Stafford, S. C., Stafford, A. M., & Triplett, R. S. (2010). The temperature dependence of the elasticity of Fe-bearing wadsleyite. *Physics of the Earth and Planetary Interiors*, *182*(1–2), 107–112. https://doi.org/10.1016/j.pepi.2010.06.014

Isaak, D. G., Gwanmesia, G. D., Falde, D., Davis, M. G., Triplett, R. S., & Wang, L. P. (2007). The elastic properties of β-Mg 2 SiO 4 from 295 to 660K and implications on the composition of Earth's upper mantle. *Physics of the Earth and Planetary Interiors*, *162*(1-2), 22–31. https://doi.org/10.1016/j.pepi.2007.02.010

Jackson, J. M., Sinogeikin, S. V., & Bass, J. D. (2000). Sound velocities and elastic properties of γ-Mg_2SiO_4 to 873 K by Brillouin spectroscopy. *American Mineralogist*, *85*(2), 296–303. https://doi.org/10.2138/am-2000-2-306

Jacobsen, S. D. (2006). Effect of water on the equation of state of nominally anhydrous minerals. *Reviews in Mineralogy and Geochemistry*, *62*(1), 321–342. https://doi.org/10.2138/rmg.2006.62.14

Jacobsen, S. D., & Van der Lee, S. (2006). *Earth's deep water cycle*. Washington DC: American Geophysical Union. https://doi.org/10.1029/GM168

Jacobsen, S. D., Jiang, F. M., Mao, Z., Duffy, T. S., Smyth, J. R., Holl, C. M., & Frost, D. J. (2008). Effects of hydration on the elastic properties of olivine. *Geophysical Research Letters*, *35*, L14303. https://doi.org/10.1029/2008GL034398

Jacobsen, S. D., Jiang, F. M., Mao, Z., Duffy, T. S., Smyth, J. R., Holl, C. M., & Frost, D. J. (2009). Correction to "Effects of hydration on the elastic properties of olivine". *Geophysical Research Letters*, *36*, L12302. https://doi.org/10.1029/2009GL038660

Jacobsen, S. D., & Smyth, J. R. (2006). Effect of water on the sound velocities of ringwoodite in the transition zone. In S. D. Jacobsen, & S. Van der Lee (Eds.), *Earth's deep water cycle* (pp. 131–145). Washington DC: American Geophysical Union. https://doi.org/10.1029/168GM10

Karato, S. (1993). Importance of anelasticity in the interpretation of seismic tomography. *Geophysical Research Letters*, *20*(15), 1623–1626. https://doi.org/10.1029/93GL01767

Karato, S. (2011). Water distribution across the mantle transition zone and its implications for global material circulation. *Earth and Planetary Science Letters*, *301*(3–4), 413–423. https://doi.org/10.1016/j.epsl.2010.11.038

Karato, S., & Jung, H. (1998). Water, partial melting and the origin of the seismic low velocity and high attenuation zone in the upper mantle. *Earth and Planetary Science Letters*, *157*(3–4), 193–207. https://doi.org/10.1016/S0012-821X(98)00034-X

Karato, S., & Spetzler, H. A. (1990). Defect microdynamics in minerals and solid-state mechanisms of seismic wave attenuation and velocity dispersion in the mantle. *Reviews of Geophysics*, *28*(4), 399–421. https://doi.org/10.1029/RG028i004p00399

Kennett, B. L. N., & Engdahl, E. R. (1991). Traveltimes for global earthquake location and phase identification. *Geophysical Journal International*, *105*(2), 429–465. https://doi.org/10.1111/j.1365-246X.1991.tb06724.x

Kennett, B. L. N., Engdahl, E. R., & Buland, R. (1995). Constraints on seismic velocities in the Earth from traveltimes. *Geophysical Journal International*, *122*(1), 108–124. https://doi.org/10.1111/j.1365-246X.1995.tb03540.x

Kohlstedt, D. L., Keppler, H., & Rubie, D. C. (1996). Solubility of water in the α, β and γ phases of $(Mg, Fe)_2SiO_4$. *Contributions to Mineralogy and Petrology*, *123*(4), 345–357. https://doi.org/10.1007/s004100050161

Komabayashi, T., & Omori, S. (2006). Internally consistent thermodynamic data set for dense hydrous magnesium silicates up to 35GPa, 1600 °C: Implications for water circulation in the Earth's deep mantle. *Physics of the Earth and Planetary Interiors*, *156*(1-2), 89–107. https://doi.org/10.1016/j.pepi.2006.02.002

Kumazawa, M., & Anderson, O. L. (1969). Elastic moduli, pressure derivatives, and temperature derivatives of single-crystal olivine and single-crystal forsterite. *Journal of Geophysical Research*, *74*(25), 5961–5972. https://doi.org/10.1029/JB074i025p05961

Li, B. S. (2003). Compressional and shear wave velocities of ringwoodite γ-Mg_2SiO4 to 12 GPa. *American Mineralogist*, *88*(8–9), 1312–1317.

Li, B. S., & Liebermann, R. C. (2000). Sound velocities of wadsleyite β-$(Mg_{0.88}Fe_{0.12})_2SiO_4$ to 10 GPa. *American Mineralogist*, *85*(2), 292–295. https://doi.org/10.2138/am-2000-2-305

Li, B. S., & Liebermann, R. C. (2007). Indoor seismology by probing the Earth's interior by using sound velocity measurements at high pressures and temperatures. *Proceedings of the National Academy of Sciences of the United States of America*, *104*(22), 9145–9150. https://doi.org/10.1073/pnas.0608609104

Li, B. S., Liebermann, R. C., & Weidner, D. J. (2001). *P-V-*V_p*-*V_s*-T* measurements on wadsleyite to 7 GPa and 873 K: Implications for the 410-km seismic discontinuity. *Journal of Geophysical Research*, *106*(B12), 30,579–30,591. https://doi.org/10.1029/2001JB000317

Liu, Q., Liu, W., Whitaker, M. L., Wang, L. P., & Li, B. S. (2008). Compressional and shear wave velocities of Fe_2SiO_4 spinel at high pressure and high temperature. *High Pressure Research*, *28*(3), 405–413. https://doi.org/10.1080/08957950802296287

Liu, W., Kung, J., & Li, B. S. (2005). Elasticity of San Carlos olivine to 8 GPa and 1073 K. *Geophysical Research Letters*, *32*, L16301. https://doi.org/10.1029/2005GL023453

Liu, W., Kung, J., Li, B. S., Nishiyama, N., & Wang, Y. B. (2009). Elasticity of $(Mg_{0.87}Fe_{0.13})_2SiO_4$ wadsleyite to 12 GPa and 1073 K. *Physics of the Earth and Planetary Interiors*, *174*(1-4), 98–104. https://doi.org/10.1016/j.pepi.2008.10.020

Liu, Z., Park, J., & Karato, S. I. (2016). Seismological detection of low-velocity anomalies surrounding the mantle transition zone in Japan subduction zone. *Geophysical Research Letters*, *43*, 2480–2487. https://doi.org/10.1002/2015GL067097

Mao, Z., Jacobsen, S. D., Frost, D. J., McCammon, C. A., Hauri, E. H., & Duffy, T. S. (2011). Effect of hydration on the single-crystal elasticity of Fe-bearing wadsleyite to 12 GPa. *American Mineralogist*, *96*(10), 1606–1612. https://doi.org/10.2138/am.2011.3807

Mao, Z., Jacobsen, S. D., Jiang, F., Smyth, J. R., Holl, C. M., & Duffy, T. S. (2008). Elasticity of hydrous wadsleyite to 12 GPa: Implications for Earth's transition zone. *Geophysical Research Letters*, *35*, L21305. https://doi.org/10.1029/2008GL035618

Mao, Z., Jacobsen, S. D., Jiang, F., Smyth, J. R., Holl, C. M., Frost, D. J., & Duffy, T. S. (2010). Velocity crossover between hydrous and anhydrous forsterite at high pressures. *Earth and Planetary Science Letters*, *293*(3–4), 250–258. https://doi.org/10.1016/j.epsl.2010.02.025

Mao, Z., & Li, X. Y. (2016). Effect of hydration on the elasticity of mantle minerals and its geophysical implications. *Science China Earth Sciences*, *59*(5), 873–888. https://doi.org/10.1007/s11430-016-5277-9

Mao, Z., Lin, J. F., Jacobsen, S. D., Duffy, T. S., Chang, Y. Y., Smyth, J. R., et al. (2012). Sound velocities of hydrous ringwoodite to 16 GPa and 673 K. *Earth and Planetary Science Letters*, *331*, 112–119.

Mayama, N., Suzuki, I., Saito, T., Ohno, I., Katsura, T., & Yoneda, A. (2005). Temperature dependence of the elastic moduli of ringwoodite. *Physics of the Earth and Planetary Interiors*, *148*(2-4), 353–359. https://doi.org/10.1016/j.pepi.2004.09.007

Minster, J. B., & Anderson, D. L. (1981). A model of dislocation-controlled rheology for the mantle. *Philosophical Transactions of the Royal Society A*, *299*(1449), 319–356. https://doi.org/10.1098/rsta.1981.0025

Ohtani, E., Litasov, K., Hosoya, T., Kubo, T., & Kondo, T. (2004). Water transport into the deep mantle and formation of a hydrous transition zone. *Physics of the Earth and Planetary Interiors*, *143*, 255–269.

Ohtani, E., Toma, M., Litasov, K., Kubo, T., & Suzuki, A. (2001). Stability of dense hydrous magnesium silicate phases and water storage capacity in the transition zone and lower mantle. *Physics of the Earth and Planetary Interiors*, *124*(1–2), 105–117. https://doi.org/10.1016/S0031-9201(01)00192-3

Pearson, D. G., Brenker, F. E., Nestola, F., McNeill, J., Nasdala, L., Hutchison, M. T., et al. (2014). Hydrous mantle transition zone indicated by ringwoodite included within diamond. *Nature*, *507*(7491), 221–224. https://doi.org/10.1038/nature13080

Pollack, H. N., Hurter, S. J., & Johnson, J. R. (1993). Heat flow from the Earth's interior: Analysis of the global data set. *Reviews of Geophysics*, *31*(3), 267–280. https://doi.org/10.1029/93RG01249

Ringwood, A. E., & Major, A. (1967). High-pressure reconnaissance investigations in the system Mg_2SiO_4-MgO-H_2O. *Earth and Planetary Science Letters*, *2*(2), 130–133. https://doi.org/10.1016/0012-821X(67)90114-8

Ritsema, J., van Heijst, H. J., & Woodhouse, J. H. (2004). Global transition zone tomography. *Journal of Geophysical Research*, *109*, B02302. https://doi.org/10.1029/2003JB002610

Romanowicz, B. A. (1979). Seismic structure of the upper mantle beneath the United States by three-dimensional inversion of body wave arrival times. *Geophysical Journal International*, *57*(2), 479–506. https://doi.org/10.1111/j.1365-246X.1979.tb04790.x

Schaeffer, A. J., & Lebedev, S. (2014). Imaging the North American continent using waveform inversion of global and USArray data. *Earth and Planetary Science Letters*, *402*, 26–41. https://doi.org/10.1016/j.epsl.2014.05.014

Schmandt, B., Jacobsen, S. D., Becker, T. W., Liu, Z. X., & Dueker, K. G. (2014). Dehydration melting at the top of the lower mantle. *Science*, *344*(6189), 1265–1268. https://doi.org/10.1126/science.1253358

Schmandt, B., & Lin, F. C. (2014). *P* and *S* wave tomography of the mantle beneath the United States. *Geophysical Research Letters*, *41*, 6342–6349. https://doi.org/10.1002/2014GL061231

Sinogeikin, S. V., Bass, J. D., & Katsura, T. (2003). Single-crystal elasticity of ringwoodite to high pressures and high temperatures: Implications for 520 km seismic discontinuity. *Physics of the Earth and Planetary Interiors*, *136*(1–2), 41–66. https://doi.org/10.1016/S0031-9201(03)00022-0

Sinogeikin, S. V., Bass, J. D., Kavner, A., & Jeanloz, R. (1997). Elasticity of natural majorite and ringwoodite from the Catherwood meteorite. *Geophysical Research Letters*, *24*(24), 3265–3268. https://doi.org/10.1029/97GL03217

Sinogeikin, S. V., Katsura, T., & Bass, J. D. (1998). Sound velocities and elastic properties of Fe-bearing wadsleyite and ringwoodite. *Journal of Geophysical Research*, *103*(B9), 20,819–20,825. https://doi.org/10.1029/98JB01819

Smyth, J. R. (1987). β-Mg_2SiO_4: A potential host for water in the mantle. *American Mineralogist*, *72*, 1051–1055.

Smyth, J. R. (1994). A crystallographic model for hydrous wadsleyite (β-Mg_2SiO_4): An ocean in the Earth's interior? *American Mineralogist*, *79*, 1021–1024.

Smyth, J. R., & Frost, D. J. (2002). The effect of water on the 410-km discontinuity: An experimental study. *Geophysical Research Letters*, *29*(10), 1485. https://doi.org/10.1029/2001GL014418

Smyth, J. R., Holl, C. M., Frost, D. J., & Jacobsen, S. D. (2004). High-pressure crystal chemistry of hydrous ringwoodite and water in the Earth's interior. *Physics of the Earth and Planetary Interiors*, *143-144*, 271–278. https://doi.org/10.1016/j.pepi.2003.08.011

Speziale, S., Duffy, T. S., & Angel, R. J. (2004). Single-crystal elasticity of fayalite to 12 GPa. *Journal of Geophysical Research*, *109*, B12202. https://doi.org/10.1029/2004JB003162

Stixrude, L., & Lithgow-Bertelloni, C. (2005). Thermodynamics of mantle minerals—I. Physical properties. *Geophysical Journal International*, *162*(2), 610–632. https://doi.org/10.1111/j.1365-246X.2005.02642.x

Stixrude, L., & Lithgow-Bertelloni, C. (2011). Thermodynamics of mantle minerals—II. Phase equilibria. *Geophysical Journal International*, *184*(3), 1180–1213. https://doi.org/10.1111/j.1365-246X.2010.04890.x

Stixrude, L., & Lithgow-Bertelloni, C. (2012). Geophysics of chemical heterogeneity in the mantle. *Annual Review of Earth and Planetary Sciences*, *40*(1), 569–595. https://doi.org/10.1146/annurev.earth.36.031207.124244

Suzuki, R., Yamaguchi, T., Li, C. L., & Klatzo, I. (1983). The effects of 5-minute ischemia in Mongolian gerbils: II. Changes of spontaneous neuronal activity in cerebral cortex and CA1 sector of hippocampus. *Acta Neuropathologica*, *60*(3-4), 217–222. https://doi.org/10.1007/BF00691869

Tenner, T. J., Hirschmann, M. M., Withers, A. C., & Ardia, P. (2012). H_2O storage capacity of olivine and low-Ca pyroxene from 10 to 13 GPa: Consequences for dehydration melting above the transition zone. *Contributions to Mineralogy and Petrology*, *163*(2), 297–316. https://doi.org/10.1007/s00410-011-0675-7

Thio, V., Cobden, L., & Trampert, J. (2016). Seismic signature of a hydrous mantle transition zone. *Physics of the Earth and Planetary Interiors*, *250*, 46–63. https://doi.org/10.1016/j.pepi.2015.11.005

Van der Hilst, R. D., Widiyantoro, S., & Engdahl, E. R. (1997). Evidence for deep mantle circulation from global tomography. *Nature*, *386*(6625), 578–584. https://doi.org/10.1038/386578a0

Van der Lee, S., & Frederiksen, A. (2005). Surface wave tomography applied to the North American upper mantle. In A. Levander & G. Nolet (Eds.), *Seismic Earth: Array analysis of broadband seismograms* (pp. 67–80). Washington, DC: American Geophysical Union.

Van der Lee, S., & Nolet, G. (1997). Upper mantle S velocity structure of North America. *Journal of Geophysical Research*, *102*(B10), 22,815–22,838.

Van der Lee, S., Regenauer-Lieb, K., & Yuen, D. A. (2008). The role of water in connecting past and future episodes of subduction. *Earth and Planetary Science Letters*, *273*(1), 15–27.

Van der Meijde, M., Marone, F., Giardini, D., & Van der Lee, S. (2003). Seismic evidence for water deep in earth's upper mantle. *Science*, *300*(5625) 1556–1558.

Wang, J. Y., Sinogeikin, S. V., Inoue, T., & Bass, J. D. (2003). Elastic properties of hydrous ringwoodite. *American Mineralogist*, *88*(10), 1608–1611. https://doi.org/10.2138/am-2003-1025

Wang, J. Y., Sinogeikin, S. V., Inoue, T., & Bass, J. D. (2006). Elastic properties of hydrous ringwoodite at high-pressure conditions. *Geophysical Research Letters*, *33*, L14308. https://doi.org/10.1029/2006GL026441

Wang, X. B., Chen, T., Zou, Y. T., Liebermann, R. C., & Li, B. S. (2015). Elastic wave velocities of peridotite KLB-1 at mantle pressures and implications for mantle velocity modeling. *Geophysical Research Letters*, *42*, 3289–3297. https://doi.org/10.1002/2015GL063436

Watt, J. P., Davies, G. F., & O'Connell, R. J. (1976). The elastic properties of composite materials. *Reviews of Geophysics*, *14*(4), 541–563. https://doi.org/10.1029/RG014i004p00541

Webb, S. L. (1989). The elasticity of the upper mantle orthosilicates olivine and garnet to 3 GPa. *Physics and Chemistry of Minerals*, *16*(7), 684–692.

Weidner, D. J. (1986). Mantle model based on measured physical properties of minerals. In S. K. Saxena (Ed.), *Chemistry and physics of terrestrial planets* (pp. 251–274). New York: Springer-Verlag. https://doi.org/10.1007/978-1-4612-4928-3_7

Wood, B. J. (1995). The effect of H_2O on the 410-kilometer seismic discontinuity. *Science*, *268*(5207), 74–76. https://doi.org/10.1126/science.268.5207.74

Xu, W. B., Lithgow-Bertelloni, C., Stixrude, L., & Ritsema, J. (2008). The effect of bulk composition and temperature on mantle seismic structure. *Earth and Planetary Science Letters*, *275*(1–2), 70–79. https://doi.org/10.1016/j.epsl.2008.08.012

Ye, Y., Brown, D. A., Smyth, J. R., Panero, W. R., Jacobsen, S. D., Chang, Y. Y., et al. (2012). Compressibility and thermal expansion of hydrous ringwoodite with 2.5(3) wt% H_2O. *American Mineralogist*, *97*(4), 573–582. https://doi.org/10.2138/am.2012.4010

Zaug, J. M., Abramson, E. H., Brown, J. M., & Slutsky, L. J. (1993). Sound velocities in olivine at Earth mantle pressures. *Science*, *260*(5113), 1487–1489. https://doi.org/10.1126/science.260.5113.1487

Zha, C. S., Duffy, T. S., Downs, R. T., Mao, H. K., & Hemley, R. J. (1996). Sound velocity and elasticity of single-crystal forsterite to 16 GPa. *Journal of Geophysical Research*, *101*(B8), 17,535–17,545. https://doi.org/10.1029/96JB01266

Zha, C. S., Duffy, T. S., Downs, R. T., Mao, H. K., & Hemley, R. J. (1998). Brillouin scattering and X-ray diffraction of San Carlos olivine: Direct pressure determination to 32 GPa. *Earth and Planetary Science Letters*, *159*(1–2), 25–33. https://doi.org/10.1016/S0012-821X(98)00063-6

Zha, C. S., Duffy, T. S., Mao, H. K., Downs, R. T., Hemley, R. J., & Weidner, D. J. (1997). Single-crystal elasticity of beta-Mg_2SiO_4 to the pressure of the 410 km seismic discontinuity in the Earth's mantle. *Earth and Planetary Science Letters*, *147*(1–4), 9–15.